Woodpile photonic crystal for beam collimation

Lina Maigyte[1], Jose Trull[1], Vygantas Mizeikis[2], Mangirdas Malinauskas[3], Saulius Juodkazis[4], Crina M. Cojocaru[1], Marius Rutkauskas[3], Martynas Peckus[5], Valdas Sirutkaitis[3] and Kestutis Staliunas[1,6]

[1]Departament de Física i Enginyeria Nuclear,Universitat Politècnica de Catalunya, Colom 11, 08222 Terrassa, Barcelona Spain

[2]Division of Global Research Leaders (Research Institute of Electronics) Shizuoka University, 3-5-1 Johoku, Naka-ku, Hamamatsu 432-8561, Japan

[3]Laser Research Center, Dep. Of Quantum Electronics, Vilnius University, Sauletekio al 10, LT-10222 Vilnius, Lithuania

[4]Swinburne University of Technology, Centre for Micro-Photonics (H38), John Street, PO Box 218, Hawthorn, Victoria , 3122, Australia

[5]Center for Physical Sciences and Technology, Savanoriu Ave. 231, LT-02300, Vilnius, Lithuania

[6]Institució Catalana de Reserca i Estudis Avançats (ICREA), Pg. Lluis Companys, 23, 08010, Barcelona, Spain

ABSTRACT

We report and analyze experimental observation of the formation of a narrow, well collimated laser beam at optical frequency behind the woodpile photonic crystal fabricated using a femtosecond laser multi-photon polymerization technique. We show that the collimation depends on the input laser beam focusing conditions. We discuss the experimental results and give theoretical interpretation.

Keywords: Photonic crystals, modulated materials, collimation, beam shaping.

1. INTRODUCTION

Photonic crystals (PhCs) are usually associated with the temporal dispersion, in particular with photonic band gaps (PBG) - ranges of frequency in which light cannot propagate in the photonic structure [1]. Temporal dispersion is the dependence of the frequency of propagation eigenmodes (Bloch modes) on the modulus of propagation wave number $\omega = \omega(|\vec{k}|)$. Recently it has been discovered that the spatial dispersion properties of PhCs can be also tailored, which allow to manage spatial propagation properties of light. In particular this can lead to appearance of angular band-gaps, which could be used for spatial (angular) filtering of propagating light [2,3]. Spatial propagation can be interpreted in terms of spatial dispersion diagrams, given by the curves of constant frequency of Bloch modes in the $\vec{k}$ space (i.e., $\omega(|\vec{k}|) = const$) or, equivalently, by $k_{\parallel}(k_{\perp})$ and by the modification of these curves by PhCs. There exist other interesting peculiarities in PhCs related with modification of spatial dispersion like vanishing of diffraction or self collimation of propagating light [4-8], it is also investigated in other fields of wave propagation, like acoustics with sonic crystals [9,10]. It is also possible to obtain negative-refraction or super-refraction of light in PhCs [11]. Most of the above listed effects refer to the propagation of the beams inside the PhCs. Less is understood about the behavior of the beams behind the crystals with nontrivial dispersion properties. The ideas have been promoted that the PhCs should show super-lensing effects [12]. So far, most of propagation effects have been studied in 2D PhCs as they are more facile to fabricate, however full control over the beam propagation can be achieved only in 3D PhCs. Nevertheless, some investigation on self-collimation in 3D PhCs at visible frequencies have been done [13,14] as well as at microwave frequencies [15] and also in the field of acoustics (with sonic crystals) [16]. In the latter two cases high resolution of fabrication for 3D structures is not required and they can be prepared by mechanical machining. In the

Photonic Crystal Materials and Devices X, edited by Hernán Ruy Míguez, Sergei G. Romanov, Lucio Claudio Andreani, Christian Seassal, Proc. of SPIE Vol. 8425, 842511 · © 2012 SPIE
CCC code: 0277-786X/12/$18 · doi: 10.1117/12.922276

paper we concentrate on the beam propagation behind the PhCs at optical (visible) frequencies and report an experimental observation of the formation of well collimated beam behind the 3D PhC of a woodpile type [17].

2. PHOTONIC CRYSTALS

Our samples of woodpile PhCs (Fig.1) were fabricated using a femtosecond laser multi-photon polymerization technique, i.e. by direct 3D writing in polymers with up to 200 nm spatial resolution. Local polymerization is achieved in photopolymerizable material via nonlinear absorption of ultrashort, tightly focused, laser pulses in the bulk of resist, resulting in tiny polymerized volume elements suspended in the resist. Using relative translation of the focal spot with respect to the sample, line traces of photopolymerized material are created, which are stable against subsequent wet development process, in which the unexposed material is washed away. As a result free-standing 3D objects anchored to the glass were fabricated. The method is described in [18-22]. The photosensitive material in our case was hybrid organic-inorganic Zr containing SZ2080 ensuring high resolution and low geometrical distortions [23]. The woodpile structures of PhCs are composed of parallel photoresist rods arranged into stacked layers. Rods in every other layer are rotated by a 90^0 angle and displaced laterally by a half of transverse lattice period (relative to the second previous layer), as illustrated in Fig.1.a. The micrograph by electronic microscope is given in Fig.1.b. Figure 1.c and Fig.1.d are the top and side images of the PhC samples, respectively.

We used two different kinds of samples: of moderate refractive index contrast and of low refractive index contrast. The low index contrast samples were obtained by filling the air voids with another polymer (polyethylene glycol) diacrylate. The low contrast samples had longitudinal period of $4.5\mu m$ while moderate contrast samples had longitudinal period of $4.1\mu m$. The transverse period was $1\mu m$ for both types of the samples. The PhCs contained 12 longitudinal modulation periods, i. e. consisted of 48 layers on a glass substrate, and are of transverse dimensions of $80\mu m$. We note that each longitudinal period period consists of 4 layers (see Fig.1.a.).

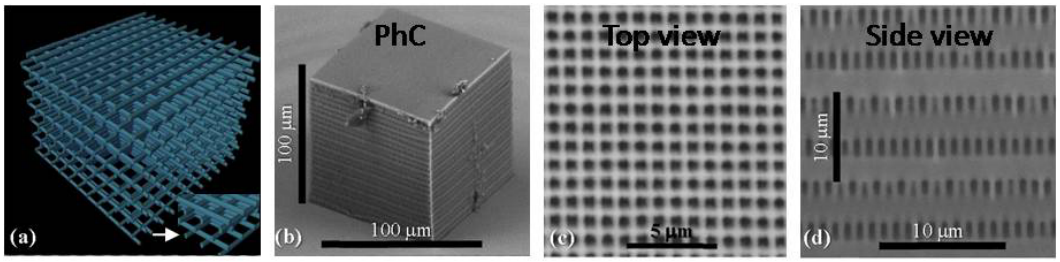

Figure 1. The woodpile PhC sample where every second layer of piles of the same orientation is shifted half-period: (a) illustration of architecture; (b) micrograph by the electronic microscope; (c) zoom of the top view; (d) side view.

3. THEORY

In order to interpret the light propagation effects we used paraxial approximation for the light propagation in a spatially modulated refraction index material:

$$\left(2ik_0\frac{\partial}{\partial z}+\nabla_\perp^2+2\Delta n(x,y,z)k_0^2\right)A(x,y,z)=0. \quad (1)$$

Here A(x,y,z) stands for the slowly varying complex envelope of the electromagnetic field in 3D space propagating along z-direction with the carrier wave number $k_0 = n\frac{\omega_0}{c}$, n is the average refraction index of the material, $\nabla_\perp^2=\frac{\partial^2}{\partial x^2}+$

$\frac{\partial^2}{\partial y^2}$ is the Laplace operator in the transverse space to the propagation direction. Relatively large spatial periods of the index variation (compared with the wavelength) justifies (1) as an acceptable approximation.

The woodpile architecture of PhCs enables reduction of the 3D paraxial wave equations into two separate 2D paraxial wave equations, as the woodpile structure consists of the bars directed along the x and y directions in alternating order. Therefore, the profile of refraction index for the woodpile PhCs can be expressed as $\Delta n(x,y,z) = \Delta n_x(x,z) + \Delta n_y(y,z)$. The reduced 2D index profiles $\Delta u_x(x,z), \Delta u_y(y,z)$ are of rhombic symmetry, and light propagation is parallel to the long diagonals of the rhombs, z. The 3D field can be factorized in the following paraxial treatment: $A(x,y,z) = A_x(x,z)A_y(y,z)$. Which inserted into (1) allows to separate the factorized components:

$$\left(2ik_0\frac{\partial}{\partial z} + \frac{\partial^2}{\partial x_i^2} + 2\Delta n_{x_i}(x_i,z)k_0^2\right)A_{x_i}(x_i,z) = 0. \tag{2}$$

Here $x_i = x, y$. To calculate the spatial dispersion curves in 2D (as well as eventually the dispersion surfaces in 3D), the harmonic expansion can be applied to each ($x_i = x, y$) of factorized components:

$$A_x(x,z) = e^{ik_z z}e^{ik_x x}\left(A_0(k_x) + \sum_{m_x,m_z} A_{m_x,m_z}(k_x)e^{im_x q_x x - im_z q_z z}\right). \tag{3}$$

We consider only the most relevant first order diffraction components $A_{m_x,m_z}(k_x)$: $(m_x,m_z) = (-1,+1),(+1,+1)$, in addition to the zero component $A_0(k_x)$: $(m_x,m_z) = (0,0)$. This truncation is justified by experimental observations as only first diffraction maxima are visible (second maxima are too weak to influence the wave propagation). Inserting the Eq. (3) into Eq. (2) gives three coupled equations for the above field components:

$$K_z A_{m_x,m_z} = \left(-\frac{(K_x + m_x Q_x)^2}{2} + m_z Q_z\right)A_{m_x,m_z} + \Delta n_0 f \sum_{l_x,l_z} A_{l_x,l_z} \cdot C_{l_x,l_z}^{m_x,m_z}. \tag{4}$$

Here Δn_0 is the refraction index contrast and f is the filling factor (the area of the polymer bar with respect to the area of the 2D cell ($f \approx 0.1$ in experiment), $K_{x,z} = \frac{k_{x,z}}{k_0}$ and $Q_{x,z} = \frac{q_{x,z}}{k_0}$ are normalized wave vector components. The coupling between harmonic components is determined by the coupling matrix $C_{l_x,l_z}^{m_x,m_z}$. The energy exchange between all three harmonic components is most efficient at the resonance $Q_x^2 - 2Q_z = 0$, as follows from Eq. (4), which means that all three dispersion lines cross at point $K_x = 0$. The resonance point in the paraxial model corresponds to the corner of a particular Brillouin zone in the full model. At the cross point, the lines deform due to the mode coupling and the positively curved segments appear, evidencing the negative diffraction of corresponding Bloch modes.

To interpret the wave propagation inside and behind the PhC we performed series of numerical simulations of (4). The variation of refractive index contrast, of longitudinal and transverse periods of the crystal is drastically affecting intensity distribution of the field as summarized in the Fig.2.a.b.c. In fact, in these figures we see the signatures of spatial beam filtering as part of distribution has dips which correspond to the diffracted components from the spatial spectrum (see more in [3] for light, in [24] for acoustics and in [25] Bose condensate waves). What is important here, are the angular distribution of the phase of transmitted wave components Fig.2.d.e.f. Numerical simulations show that normally the phase shift profile obtain negative curvatures, as in the cases of Fig.2.d and Fig.2.e (indicated by arrows). In Fig.2.f we notice positive curvature of dispersion curve. It is very peculiar as positive curvature in this case is responsible for the negative diffraction of the beams inside the PhC and therefore it is a key feature which leads to the beam collimation behind the PhCs. So the simulated PhC for the case of Fig.2.c,f should show a collimation of the beams behind the PhC. PhCs were fabricated taking into account simulated positive diffraction curves.

The negative diffraction inside the PhC governs the collimation of the beam behind the PhCs in the way that it compensates the diffractive broadening of the beam propagating in space before it reaches the front face of the PhC.

Inside this type of PhC as the diffractive broadening is compensated, therefore at the back face of the PhC the beam wave fronts are flat and when it pass the PhC the beam continues propagating well collimated.

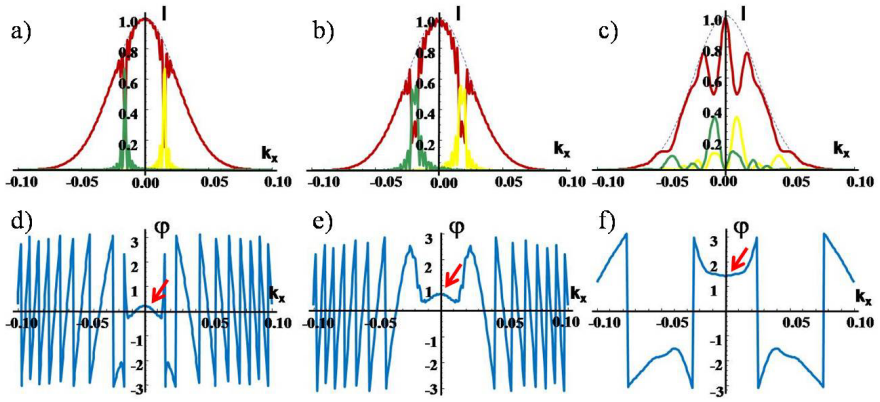

Figure 2. Series of numerical simulations of plane wave propagation in PhCs depending on incidence angle k_x: (a,b,c) the intensity distributions of the beam in a far field and first diffraction components (green and yellow curves). All three cases were simulated for slightly different PhC parameters; (d,e,f) The phase shifts corresponding to intensity distributions above. The cases of (d,e) show usual negatively curved phase segment in the dispersion curve, while (f) show positive curvature which corresponds to the negative diffraction inside PhC.

The negative diffraction in the PhC depends on the parameters (spatial periods and modulation) of the PhC, therefore the optimum collimation of the beams depend on the distance between the focal plane of the beam and the PhC. We made series of numerical calculations by integrating 2D version of paraxial propagation equation (1) (Fig. 3). In Fig.3.c formation of well collimated beams in 2D case is obtained.

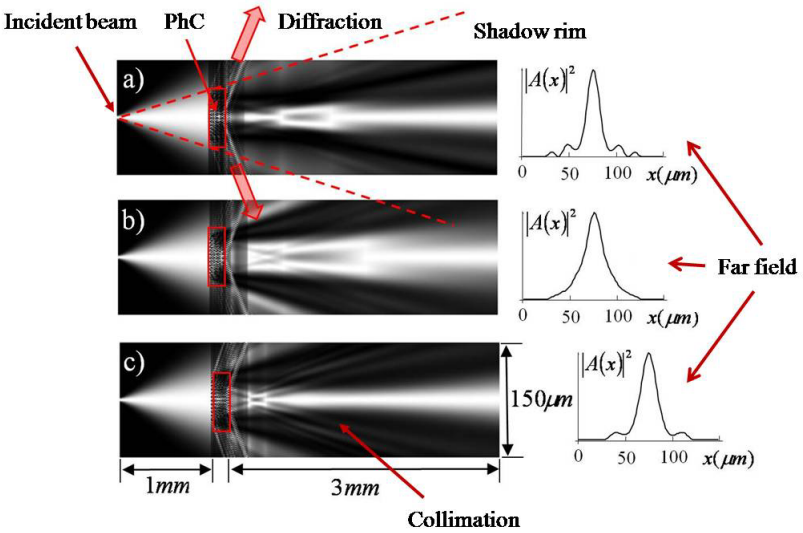

Figure 3. Beam propagation inside and behind the PhC for three cases with slightly different parameters as obtained by numerical integration of the paraxial model (2) in 2D. The one dimensional (1D) profiles of beam in the far-field are shown on the right.

4. RESULTS

The reported experimental observation is illustrated in Fig.4. In experiments the Nd:YAG laser beam of $\lambda = 532nm$ is tightly focused by x10 microscope objective (numerical aperture NA=0.25) and the woodpile PhC is positioned at some

distance behind the focal plane of the beam, the distribution of intensity in the far field could be observed in the screen or CCD camera which were placed at approximately 5cm behind the PhC (Fig.4.a).

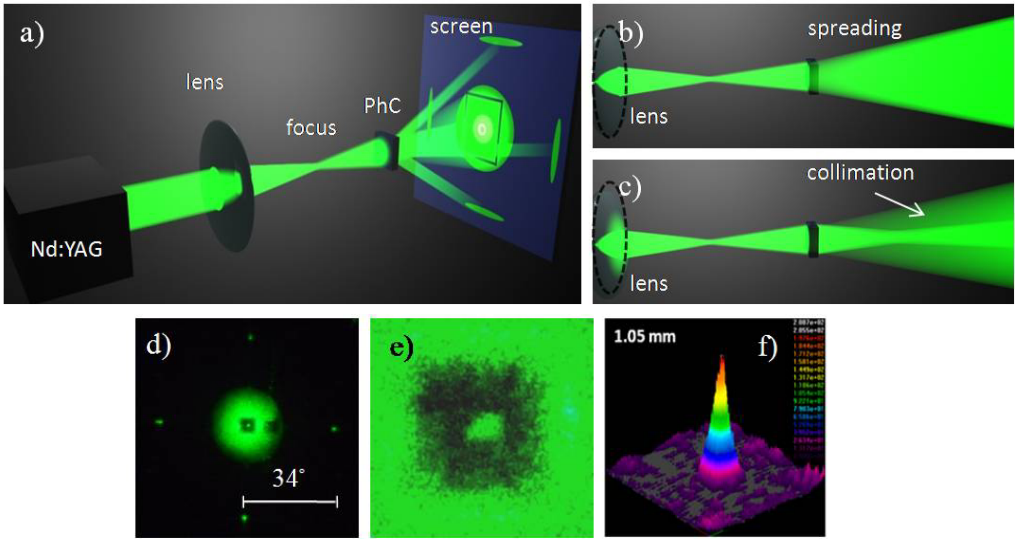

Figure 4. (a) Experimental scheme; (b) Light propagation behind the sample without any beam shaping properties, where the beam is spreading in a usual way in free propagation; (c) Light propagation behind the PhC with negative diffraction properties, where collimation of the beam in the central part of the beam in the propagation direction is obtained; (d) the snapshot of far field distribution on the screen (large spatial scale) where shadow of the moderate contrast PhC sample with the relatively round spot in the middle is obtained. Four first order diffraction maxima at angles of 34 are seen as well; (e) zoom of the shadow of the crystal from the previous distribution where relatively round spot is obtained and which is corresponding to the collimated beam behind the PhC; (f) snapshot made by the CCD camera of the collimated beam (on small spatial scale).

In Fig.4.b we illustrate the case how the light would propagate behind PhC if it wouldn't have any beam shaping properties. In Fig.4.c it is illustrated how the beam propagates behind the PhC characterized by negative diffraction. We expect that some part of light is collimated in propagation. Fig.4.d shows the far-field intensity distribution as taken with the camera. On the screen in the middle of the beam we observe the shadow of the sample (Fig.4.e the zoom of central part of Fig.4.d) which appears due to the scattering of the light by the PhC and four first order diffraction maxima of the incident beam. The diffraction angles are of $34^0$and 31^0 for moderate and low contrast samples respectively, and fit well with those calculated from the transverse period of the PhCs. Most importantly, at the middle of the shadow a relatively round spot is clearly seen, which corresponds to a well collimated beam behind the PhC. In Fig.4.f the snapshot of the collimated beam in the middle of the shadow of the PhC is displayed by CCD camera. Making series of measurements by CCD camera we noticed that the shape and the intensity of the spot depend on the distance between the focal plane and the crystal. Fig.5 gives summarized quantitative results of observation for both types of samples. It shows that the optimum distance for optimum collimation of the beam between the focal plane and the PhC sample is 1mm for the moderate index contrast PhC and 4mm form the low index contrast PhC sample. Moreover, it is important to mention that the top intensities of the spot significantly exceeded the irradiation intensity by approximately 2 and 22 times for moderate and for low index contrast PhC samples respectively.

It is important to mention that when the PhC sample is being slightly tilted (within 2^0) the spot remains at the middle of the shadow. This observation excludes all possible interpretations of the effect by the reflections from the surfaces of the sample as well as by a light guiding along the lateral facets.

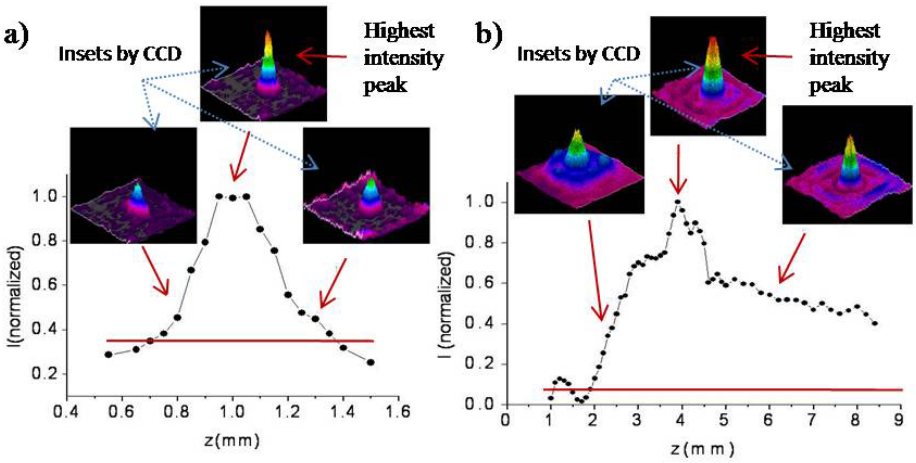

Figure 5. Top intensity of the collimated beam depending on the distance between the focal plane and the PhC for the moderate contrast (a) and low contrast (b) sample. The typical shapes of the beam for different positions of the PhC relative to the focal plane are indicated by the insets. The intensity of light without the PhC is marked by the thin horizontal red line for both of the cases.

5. CONCLUSION

We report the experimental observation of a collimation of diverging incident light beam by a 3D photonic crystal of a woodpile type. The efficiency of the beaming in experiments reached only 20% (in terms of the energy part collected into a beam), which is close to the theoretically estimated value. However, the special measures can be taken in order to project the radiation more efficiency. This gives hope to improve the performance of the beamer. Finally, we note that physical mechanisms of the beam formation can be generally applied to the other types of waves in periodic structures, e.g. to acoustic waves in sonic crystals, surface polariton waves, and others.

ACKNOWLEDGEMENTS

The work was financially supported by Spanish Ministerio de Ciencia e Innovación and European Union FEDER through projects FIS2008-06024-C03-C02, and FIS2011-29731-C02-01, by EC Seventh Framework Programme LASERLAB-EUROPE (grant agreements n° 228334), and by European Union Structural Funds project "Postdoctoral Fellowship Implementation in Lithuania".

REFERENCES

[1] Yablonovitch, E., "Inhibited spontaneous emission in solid-state physics and electronics," Phys. Rev. Lett. **58**, 2059-2062 (1987).
[2] Staliunas, K., and Sánchez-Morcillo, V.J., "Spatial filtering of light by chirped photonic crystals," Phys. Rev. A **79**, 053807-053812 (2009).
[3] Maigyte, L., Gertus, T., Trull, J., Cojocaru, C., Sirutkaitis, V., and Staliunas, K., "Signatures of light-beam spatial filtering in a three-dimensional photonic crystal," Phys. Rev. A **82,** 043819-043823 (2010).
[4] Zengerle, R., "Light propagation in singly and doubly periodic planar waveguides," J. Mod. Opt. **34**, 1589-1617 (1987).
[5] Kosaka, H., Kawashima, T., Tomita, A., Notomi, M., Tamamura, T., Sato, T., and Kawakami, S., "Self-collimating phenomena in photonic crystals," Appl. Phys. Lett. **74**, 1212-1214 (1999).
[6] Dholakia, K., and Reece, P., "Optical micromanipulation takes hold," Nanotoday **1**, 18-27 (2006).
[7] Chigrin, D. N., Enoch, S., Torres, C. S., and Tayeb, G., "Self-guiding in two-dimensional photonic crystals," Opt. Express **11**, 1203-1211 (2003).

[8] Staliunas, K., and Herrero, R., "Nondiffractive propagation of light in photonic crystals," Phys. Rev. E, **73**, 01660-016606, (2006).
[9] Pérez-Arjona, I., Redondo, F., Sánchez-Morcillo, V.J., Espinosa, V., and Staliunas, K., "Theoretical prediction of the nondiffractive propagation of sonic waves through periodic acoustic media," Phys. Rev. B **75**, 014304-014310 (2007).
[10] Espinosa, V., Sanchez-Morcillo, V.J. Staliunas, K., Perez-Arjona, I., and Redondo, J., "Subdiffractive propagation of ultrasound in sonic crystals," Phys. Rev. B **76**, 140302(R)-140305 (2007).
[11] Lupu, A., de Lustrac, A., Ourir, A., Checoury, X., Lourtioz, J.M., Centeno, E., Cassagne, D., Albert, J.P., Pommereau, F., Legouezigou, L., Drisse, O., Legouezigou, O., Deroin, E., and Duan, G.H., "Discontinuous wavelength super-refraction in photonic crystal superprism," Opt. Exp **14**, 2003-2013 (2006).
[12] Cubukcu, E., Aydin, K., Ozbay, E., Foteinopoulou, S., and Soukulis, C. M., "Subwavelenght resolution in a two-dimensional photonic-crystal-based-superlens," Phys. Rev. Lett. **91**, 207401-207404 (2003).
[13] Illiew, R., Etrich, C., Peschel, U., Lederer, F., Augustin, M., Fuchs, H.-J., Schelle, D., Kley, E.-B., Nolte, S., and Tunnermann, A., "Diffractionless propagation of light in a low-index photonic-crystal film," Appl. Phys. Lett. **85**, 5854-5856 (2004).
[14] Shin, J., and Fran, S., "Conditions for slef-collimation in three-dimensional photonic crystals," Opt. Lett. **30**, 2397-2399 (2005).
[15] Lu, Z., Shi, S., Murakovski, J.A., Shneider, G.J., Schuetz, C.A., and Prather, D.W., "Experimental Demonstration of Self-Collimation inside a Three-Dimensional Photonic Crystal," Phys. Rev. Lett. 96, 173902-17390 (2006).
[16] Soliveres, E., Espinosa, V., Perez-Arjona, I., Sanchez-Morcillo V.J., and Staliunas, K., "Self collimation of ultrasound in a three-dimensional sonic crystal," Appl. Phys. Lett. **94**, 164101-164103 (2009).
[17] Trull, J., Maigyte, L., Mizeikis, V., Malinauskas, M., Juodkazis, S., Cojocaru, C., Rutkauskas, M., Peckus, M., Sirutkaitis, V., and Staliunas, K., "Formation of collimated beams behind the woodpile photonic crystal," Phys. Rev. A **84**, 033812-033816 (2011).
[18] Serbin, J., Ovsianikov, A., and Chichkov, B.N., "Fabrication of woodpile structures by two-photon polymerization and investigation of their optical properties," Optics Express **12**, 5221-5228 (2004).
[19] Deubel, M., von Freymann, G., Wegener, M., Pereira, S., Busch, K., and Soukoulis, K.M., "Direct laser writing of three-dimensional Photonic crystal-crystal tamplates for telecommunications," Nature Materials **3**, 444 (2004).
[20] Mizeikis, V., Seet, K.K., Juodkazis, S., and Misawa, H., "Three-dimensional woodpile Photonic crystal templates for the infrared spectral range," Opt. Lett. **29**, 2061-2063 (2004).
[21] LaFratta, C.N., Fourkas, J.T., Baldacchini, T., and Farrer, R.A., "Multiphoton Fabrication" ChemInform **38**, 6238–6258, (2007).
[22] Ovsianikov, A., Viertl, J., Chichkov, B., Oubaha, M., MacCraith, B., Sakellari, I., Giakoumaki, A., Gray, D., Vamvakaki, M., Farsari, M., and Fortakis, C., "Ultra-low Shrinkage Hybrid Photosensitive material for two-photon Polymerization Microfacbrication, " ACS Nano **2**, 2257-2262 (2008).
[23] Malinauskas, M., Zukauskas, A., Bickauskaite, G., Gadonas R., and Juodkazis, S., "Mechanisms of three-dimensional structuring of photo-polymers by tightly focused femtosecond laser pulses," Optics Express **18**, 10209 (2010).
[24] Picó, R., Sánchez-Morcillo, V.J., Pérez-Arjona, I., and Staliunas, K., "Spatial Filtering of Sound Beams by Sonic Crystals, Applied Acoustics," Appl. Acoust. **73,** 302-306 (2012).
[25] Staliunas, K., "Removal of excitations of Bose-Einstein condensates by space- and time-modulated potentials," Phys. Rev. A, **84**, 013626-013630 (2011).